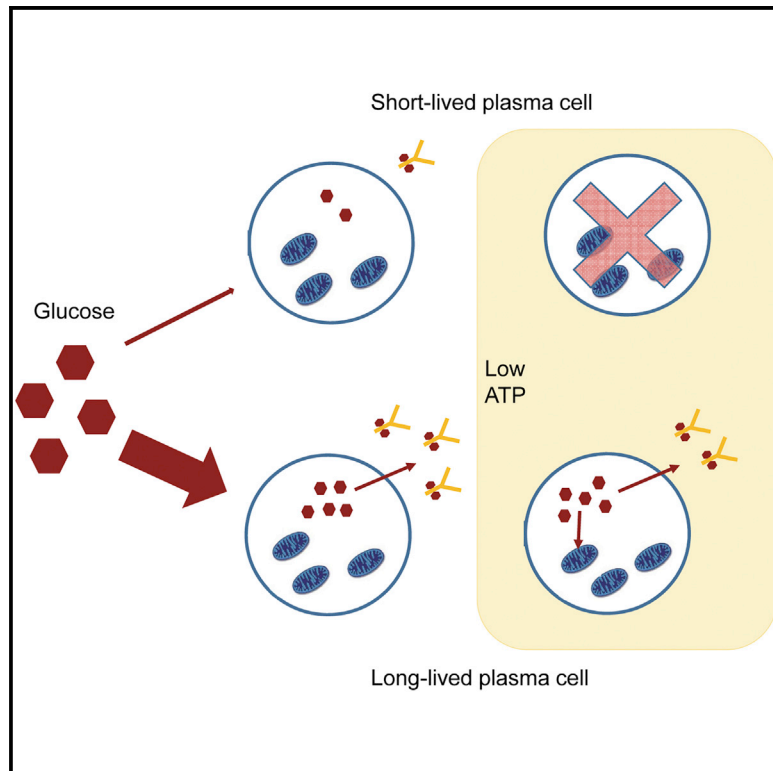


Immunity

Mitochondrial Pyruvate Import Promotes Long-Term Survival of Antibody-Secreting Plasma Cells

Graphical Abstract



Authors

Wing Y. Lam, Amy M. Becker, Krista M. Kennerly, ..., Brian N. Finck, Erika L. Pearce, Deepta Bhattacharya

Correspondence

deeptab@wustl.edu

In Brief

Durable antibody production after vaccination or infection is mediated by long-lived plasma cells (LLPCs), but specific pathways that allow LLPC persistence are unknown. Bhattacharya and colleagues show that LLPCs import and use glucose for antibody glycosylation, but in times of metabolic stress, they divert glucose to generate pyruvate for survival.

Highlights

- LLPCs import more glucose than do short-lived plasma cells (SLPCs)
- LLPCs primarily use glucose to glycosylate antibodies
- Under metabolic stress, LLPCs but not SLPCs divert glucose to form pyruvate
- Genetic ablation of mitochondrial pyruvate import shortens the lifespan of LLPCs

Accession Numbers

GSE81443



Mitochondrial Pyruvate Import Promotes Long-Term Survival of Antibody-Secreting Plasma Cells

Wing Y. Lam,^{1,10} Amy M. Becker,^{1,7,10} Krista M. Kennerly,^{1,10} Rachel Wong,¹ Jonathan D. Curtis,^{1,8} Elizabeth M. Llifrio,² Kyle S. McCommis,³ Johannes Fahrman,^{4,9} Hannah A. Pizzato,¹ Ryan M. Nunley,⁵ Jieun Lee,⁶ Michael J. Wolfgang,⁶ Gary J. Patti,² Brian N. Finck,³ Erika L. Pearce,^{1,8} and Deepta Bhattacharya^{1,*}

¹Department of Pathology and Immunology, Washington University School of Medicine, Saint Louis, MO 63110, USA

²Department of Chemistry, Washington University School of Medicine, Saint Louis, MO 63110, USA

³Center for Human Nutrition, Washington University School of Medicine, Saint Louis, MO 63110, USA

⁴West Coast Metabolomics Center, University of California, Davis, Davis, CA 95616, USA

⁵Washington University Orthopedics, Barnes Jewish Hospital, Saint Louis, MO 63110, USA

⁶Department of Biological Chemistry, Center for Metabolism and Obesity Research, Johns Hopkins University School of Medicine, Baltimore, MD 21205, USA

⁷Present address: Program in Cellular and Molecular Medicine, Boston Children's Hospital, Boston, MA 02115, USA

⁸Present address: Max Planck Institute of Immunobiology and Epigenetics, Freiburg 79108, Germany

⁹Present address: MD Anderson Cancer Center, Houston, TX 77030, USA

¹⁰Co-first author

*Correspondence: deeptab@wustl.edu

<http://dx.doi.org/10.1016/j.immuni.2016.06.011>

SUMMARY

Durable antibody production after vaccination or infection is mediated by long-lived plasma cells (LLPCs). Pathways that specifically allow LLPCs to persist remain unknown. Through bioenergetic profiling, we found that human and mouse LLPCs could robustly engage pyruvate-dependent respiration, whereas their short-lived counterparts could not. LLPCs took up more glucose than did short-lived plasma cells (SLPCs) *in vivo*, and this glucose was essential for the generation of pyruvate. Glucose was primarily used to glycosylate antibodies, but glycolysis could be promoted by stimuli such as low ATP levels and the resultant pyruvate used for respiration by LLPCs. Deletion of *Mpc2*, which encodes an essential component of the mitochondrial pyruvate carrier, led to a progressive loss of LLPCs and of vaccine-specific antibodies *in vivo*. Thus, glucose uptake and mitochondrial pyruvate import prevent bioenergetic crises and allow LLPCs to persist. Immunizations that maximize these plasma cell metabolic properties might thus provide enduring antibody-mediated immunity.

INTRODUCTION

During the initial stages of a T cell-dependent antibody response, a subset of antigen-specific B cells proliferates in the extrafollicular regions of spleens and lymph nodes to become short-lived antibody-secreting plasmablasts and plasma cells (Fagraeus, 1948; Sze et al., 2000). These cells are thought to survive for

only several days before undergoing apoptosis (Jacob et al., 1991; Smith et al., 1994; Sze et al., 2000). Other antigen-specific B cells initiate germinal center reactions where affinity maturation occurs (Berek et al., 1991). Affinity-matured germinal center B cells survive to become either memory B cells or long-lived plasma cells (LLPCs) residing mostly in the bone marrow (Benner et al., 1981).

LLPCs can live for years after infection or vaccination (Amanna et al., 2007; Manz et al., 1997; Slifka et al., 1998). These LLPCs secrete several thousand antibody molecules per second irrespective of the presence of antigen (Ahuja et al., 2008; Cambridge et al., 2003; DiLillo et al., 2008; Hibi and Dosch, 1986; Manz et al., 1998). The quantity, specificity, and duration of serum antibody production by LLPCs are the major correlates of protection for most clinically used vaccines (Amanna and Slifka, 2011). Yet the lack of durability has been a problem in certain vaccines, as was observed in the recent RTS,S/AS01E malaria clinical trial (Olotu et al., 2013). A number of intrinsic plasma cell survival molecules have been identified (O'Connor et al., 2004; Peperzak et al., 2013; Rozanski et al., 2011; Shapiro-Shelef et al., 2005; van Sriel et al., 2012), but each of these are similarly expressed between LLPCs and short-lived plasma cells (SLPCs) (Shi et al., 2015). Because the survival and metabolic pathways that specifically regulate LLPC survival remain largely unknown, optimization of the durability of vaccine-mediated immunity remains a major challenge.

As B cells differentiate into plasma cells, profound metabolic changes occur. Activated B cells increase cell surface expression of the glucose transporter Glut1 and undergo mechanistic target of rapamycin complex 2-dependent proliferation (Caro-Maldonado et al., 2014; Doughty et al., 2006; Dufort et al., 2007; Lee et al., 2013; Woodland et al., 2008). Glucose uptake is used to fuel glycolysis, electron transport chain activity, and synthesis of lipids for expansion of the endoplasmic reticulum (Dufort et al., 2014; Garcia-Manteiga et al., 2011). X-box

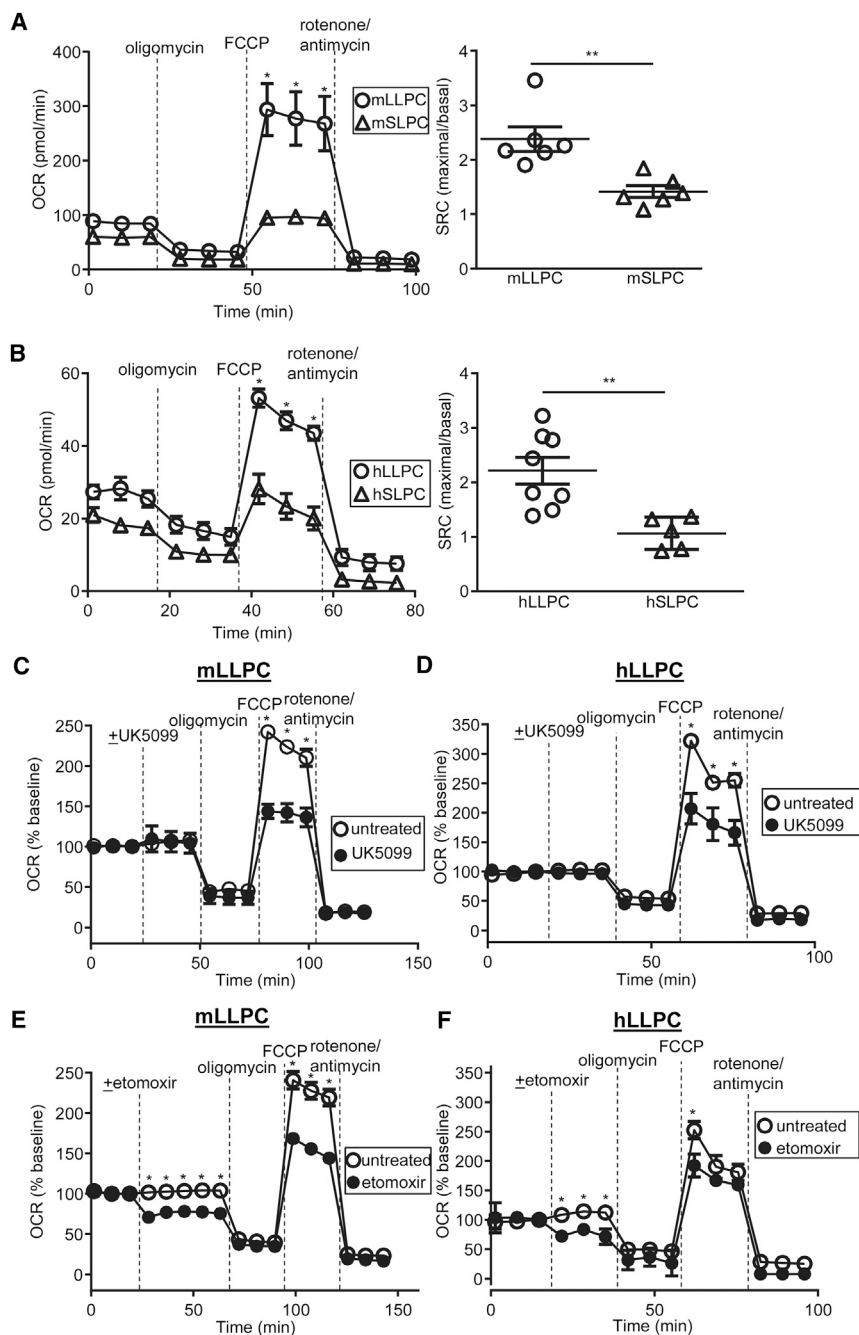


Figure 1. LLPCs Have Greater Mitochondrial Respiratory Capacity Than Do SLPCs

(A) Extracellular flux analysis of mouse splenic SLPCs (mSLPC) from immunized mice and long-lived bone marrow plasma cells (mLLPC). Oxygen consumption rates (OCR) before and after addition of pharmacological inhibitors are shown. Mean values of technical replicates \pm SEM of a representative experiment are shown in the left panel, while mean values \pm SEM of five independent experiments are shown in the right panel. * $p < 0.05$, ** $p < 0.005$ by Student's two-tailed t test.

(B) Extracellular flux analysis of human tonsillar plasma cells (hSLPC) and bone marrow plasma cells (hLLPC). Mean values of technical replicates \pm SEM of a representative experiment are shown in the left panel, while mean values \pm SEM of five independent experiments are shown in the right panel. Each symbol in the right panel represents a biologically distinct sample. * $p < 0.05$, ** $p < 0.005$ by Student's two-tailed t test.

(C and D) OCR of LLPC after inhibition of mitochondrial pyruvate transport. Mouse (C) or human (D) LLPC were left untreated or treated with 10 μ M UK5099, and OCR was measured after addition of oligomycin, FCCP, and rotenone/antimycin. Plots are representative of three independent experiments. Mean values of technical replicates \pm SEM are shown. OCR values are normalized to the reading just before the first drug injection. * $p < 0.05$, by Student's two-tailed t test.

(E and F) OCR of mouse (E) or human (F) LLPC after inhibition of fatty acid oxidation. LLPC were left untreated or treated with 200 μ M etomoxir. Plots are representative of three independent experiments. Mean values of technical replicates \pm SEM are shown. OCR values are normalized to the reading just before the first drug injection. * $p < 0.05$, by Student's two-tailed t test. See also Figure S1.

RESULTS

LLPCs but Not SLPCs Can Engage Pyruvate-Dependent Respiration

We hypothesized that to maintain their remarkable rate of antibody production, LLPCs use unique metabolic pathways unavailable to their short-lived counterparts. We measured mitochondrial oxygen

consumption rates in mouse B220⁺CD138^{high} bone marrow cells, which are enriched for LLPCs (Chernova et al., 2014), and B220^{low}CD138^{high} splenic cells isolated 7 days after immunization with 4-hydroxy-3-nitrophenyl-chicken gamma globulin (NP-CGG), which are enriched for SLPCs (Smith et al., 1994) (Figure S1A). Basal rates of oxygen consumption were similar between LLPCs and SLPCs (Figure 1A). Addition of oligomycin, an inhibitor of ATP synthase, led to a similar decline in oxygen consumption rates in LLPCs and SLPCs (Figure 1A). However, addition of the ionophore carbonyl cyanide-4-(trifluoromethoxy)phenylhydrazone (FCCP) led to a much higher maximal oxygen consumption rate by LLPCs than by SLPCs (Figure 1A).

binding protein 1 drives expression of mitochondrial and endoplasmic reticulum biosynthesis and stress-related genes (Jang et al., 2015; Shaffer et al., 2004; van Anken et al., 2003). By providing metabolic substrates, autophagy is also important for plasma cells (Pengo et al., 2013). Yet it is unclear whether specific metabolic pathways functionally differentiate LLPCs from SLPCs. In other cell types such as neurons and memory T cells, maximal respiratory capacity correlates with longevity (Choi et al., 2009; van der Windt et al., 2012). Here, we established mitochondrial pyruvate import as a critical metabolic pathway that distinguished SLPCs from LLPCs and was essential for the durability of antibody-mediated immunity.

NP-binding SLPCs also showed low maximal respiration (Figure S1B). Human bone marrow LLPCs also had more maximal respiratory capacity than did tonsillar SLPCs (Figures 1B, S1C). Addition of the electron transport chain inhibitors rotenone and antimycin A led to a complete block of oxygen consumption (Figures 1A and 1B). These results indicated that LLPCs had greater maximal respiratory capacity than SLPCs.

We next sought to identify metabolic pathways that support the elevated maximal respiratory capacity of LLPCs. Addition of UK5099, an inhibitor of mitochondrial pyruvate import, had no immediate effect on respiration but markedly attenuated maximal respiratory capacity after FCCP treatment in both mouse and human LLPCs, leaving them with a metabolic profile similar to that of SLPCs (Figures 1C and 1D). In contrast, addition of etomoxir, an inhibitor of long-chain fatty acid (LCFA) transport into the mitochondria, attenuated both basal and maximal respiration in mouse and human LLPCs (Figures 1E and 1F). Combined addition of UK5099 and etomoxir led to an additive inhibition of maximal respiration (Figure S1D). Etomoxir treatment of SLPCs also attenuated respiration, while UK5099 inhibited the small increase in respiratory capacity after FCCP treatment (Figure S1E). Inhibition of amino acid catabolism had no immediate effect on respiration in LLPCs (Figures S1F and S1G). These data demonstrated that the relative ability to engage pyruvate-dependent respiration distinguished LLPCs from SLPCs.

Mitochondrial Pyruvate Import Is Essential for Maintenance of LLPCs In Vivo

Pyruvate-dependent respiration was observed only after treatment with FCCP in vitro. Thus, it remained unclear whether this pathway is ever used by LLPCs. To address this point, we observed that in the absence of cytokines, LLPCs exhibited enhanced survival rates relative to SLPCs in vitro, but this advantage was eliminated upon treatment with UK5099 (Figure 2A). The molecular target of UK5099 is the mitochondrial pyruvate carrier composed of Mpc1 and Mpc2, each of which is essential for its function (Bricker et al., 2012; Herzig et al., 2012). To assess the importance of plasma cell mitochondrial pyruvate in vivo, we used *Mpc2^{fl/fl}* mice (McCommis et al., 2015), as constitutive deletion of *Mpc2* is embryonically lethal (Vigueira et al., 2014). Competitive bone marrow chimeras were made with CD45.1⁺ wild-type and CD45.2⁺ *Mpc2^{fl/fl}* or *Mpc2^{fl/fl}:ROSA26 CreER* donors, which express tamoxifen-inducible Cre recombinase under a constitutive promoter (Figure 2B). No differences were observed in B cell contribution between CD45.2⁺ *Mpc2^{fl/fl}* and *Mpc2^{fl/fl}:ROSA26 CreER* donors prior to tamoxifen treatment (Figure 2C). Two weeks after tamoxifen treatment, follicular B cell chimerism was unaffected by deletion of *Mpc2* (Figures 2D and 2E, S2A), despite efficient removal of the gene (Figure S2B). In contrast, *Mpc2*-deficient LLPC frequency was substantially diminished relative to control chimeras (Figures 2D and 2E). This was likely an underestimate of the requirement for mitochondrial pyruvate import, as residual LLPCs showed evidence of incomplete deletion of *Mpc2* (Figure S2B). Nonetheless, we observed a reduction in maximal respiratory capacity in *Mpc2*-deficient bone marrow plasma cells (Figure S2C). Because SLPCs persist for only 1–3 days in vivo (Sze et al., 2000), we were unable to quantify effects on the lifespans of these cells in this system. However, UK5099 did not markedly accelerate

SLPC death in vitro (Figure 2A). These data suggest that LLPCs, but not SLPCs or naive B cells, utilized mitochondrial pyruvate import to persist.

Loss of LLPCs would be predicted to lead to a decline in antigen-specific antibody titers after vaccination. To test this, we mixed wild-type immunoglobulin H^a (IgH^a) allotype cells with IgH^b *Mpc2^{fl/fl}* or *Mpc2^{fl/fl}:ROSA26 CreER* bone marrow and transplanted them into irradiated recipients (Figure 2F). Chimeras were vaccinated against West Nile virus (WNV), antigen-specific LLPCs were allowed to form over the course of 6 weeks (Purtha et al., 2011), and mice were treated with tamoxifen. No differences were observed in control WNV-specific serum IgG2a^a titers between *Mpc2^{fl/fl}* and *Mpc2^{fl/fl}:ROSA26 CreER* chimeras (Figure 2G, left panel). In contrast, at 2 and 6 weeks post-tamoxifen treatment, *Mpc2^{fl/fl}:ROSA26 CreER* chimeras showed a sharp reduction in WNV-specific IgG2a^b titers relative to *Mpc2^{fl/fl}* chimeras (Figure 2G, right panel). At 22 weeks post-vaccination, WNV envelope-specific IgG2a^b antibody-secreting cells were still reduced in *Mpc2^{fl/fl}:ROSA26 CreER* chimeras relative to controls (Figure 2H). These data demonstrated an intrinsic requirement for mitochondrial pyruvate metabolism to maintain LLPCs and antigen-specific antibodies in vivo.

Given the requirement for Mpc2 in LLPCs, we considered the possibility that plasma cells use pyruvate as the major carbon source for respiration in vivo, in contrast to our in vitro results (Figures 1C–1F). We pretreated mice with UK5099 or etomoxir and intravenously injected a methyl ester of tetramethylrhodamine (TMRM), a dye that reports mitochondrial membrane potential (Scaduto and Grotyohann, 1999). TMRM staining is reduced by a loss of respiratory substrates both in culture and in vivo (Hall et al., 2013; Vander Heiden et al., 2001). Treatment with etomoxir consistently reduced the mean fluorescent intensity (MFI) of TMRM staining in bone marrow plasma cells, indicating that LCFAs serve as basal respiratory substrates (Figure 3A). UK5099 caused a reduction in mitochondrial membrane potential in a subset of bone marrow cells, but had no reproducible effect on the MFI of TMRM staining of plasma cells (Figure 3B). To confirm these results genetically, we injected TMRM into *Mpc2^{fl/fl}:ROSA26 CreER* or control chimeras treated with tamoxifen. No differences in TMRM MFI were observed between donor and residual wild-type host bone marrow plasma cells (Figure 3C). These results indicated that LCFAs played a major role in basal LLPC respiration in vivo.

To reconcile the contribution of LCFAs to respiration with the requirement for mitochondrial pyruvate in LLPC maintenance in vivo, we hypothesized that these two types of substrates play non-redundant roles. To test this hypothesis, we transduced hematopoietic stem and progenitor cells from CD45.2⁺ *Mpc2^{fl/fl}:ROSA26 CreER* mice with retroviruses and transplanted them competitively into irradiated CD45.1⁺ recipients (Figure 3D). Retroviral expression of Mpc2 specifically protected plasma cells from deletion of endogenous *Mpc2* (Figures 3D, S3A). As expected (O'Connor et al., 2004; Peperzak et al., 2013), anti-apoptotic protein Myeloid cell leukemia 1 (Mcl1) expression promoted overall plasma cell survival, but did not confer specific protection against *Mpc2* deficiency (Figure 3D). Solute carrier 27a1 (Slc27a1), a plasma membrane LCFA transporter (Schaffer and Lodish, 1994), is not endogenously expressed by LLPCs but retroviral expression promoted uptake

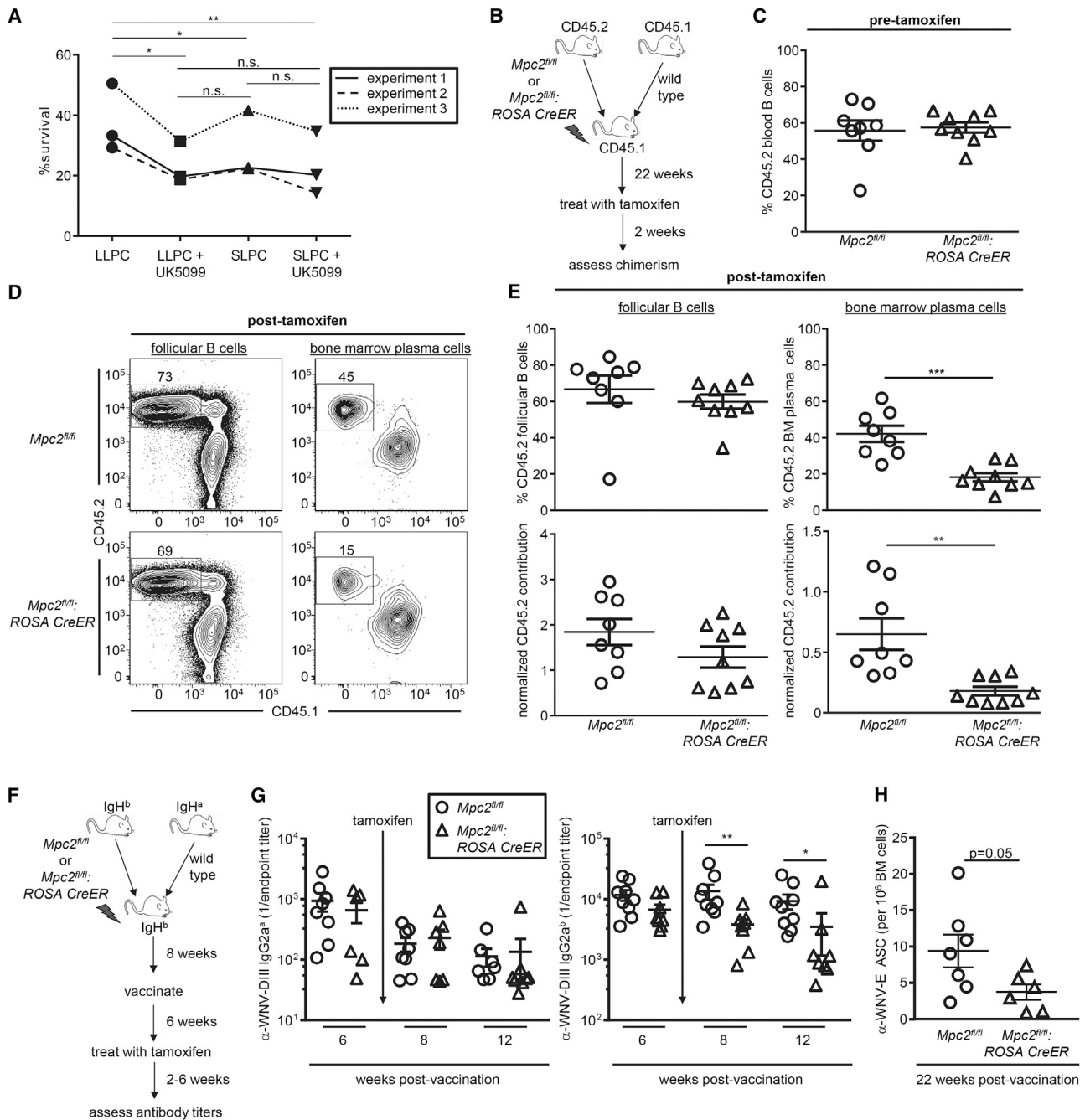


Figure 2. Mitochondrial Pyruvate Transport Is Essential for Maintenance of LLPCs In Vivo

(A) Survival of LLPCs and SLPCs in vitro. LLPCs or SLPCs from immunized mice were cultured in the presence or absence of UK5099 for 3 days. The numbers of surviving cells relative to the input are shown for three independent experiments. * $p < 0.05$, ** $p < 0.005$ by paired one-way ANOVA.

(B) Representation of mixed bone marrow chimera experiment to assess polyclonal LLPC dependence on *Mpc2*.

(C) Peripheral blood B cell chimerism prior to tamoxifen treatment. Each symbol represents a distinct mouse. Mean values \pm SEM are shown, and data are cumulative from two independent experiments.

(D) Representative plots showing CD45.2 chimerism in naive follicular B cells and bone marrow plasma cells from chimeras 2 weeks after tamoxifen injection.

(E) Cumulative chimerism data from two independent experiments. Each symbol represents a distinct mouse. Mean raw chimerism values \pm SEM (top panels) or normalized to the initial peripheral blood B cell chimerism before tamoxifen injection (bottom panels) are shown. ** $p < 0.005$, *** $p < 0.0005$ by Student's two-tailed t test.

(F) Representation of mixed bone marrow chimera experiment to assess requirement for *Mpc2* in maintaining antigen-specific antibody titers.

(G) WNV DIII-specific IgG2a^a and IgG2a^b serum antibody titers before and after tamoxifen injection. Mean endpoint titers \pm SEM are shown; each symbol represents an individual mouse. Data are cumulative from two independent experiments. * $p < 0.05$, ** $p < 0.005$ by Mann-Whitney rank test.

(H) WNV envelope-specific IgG2a^b antibody secreting cells (ASC). Mean frequencies \pm SEM are shown; each symbol represents an individual mouse. Data are cumulative from two independent experiments. $p = 0.05$ by Student's two-tailed t test. See also Figure S2.

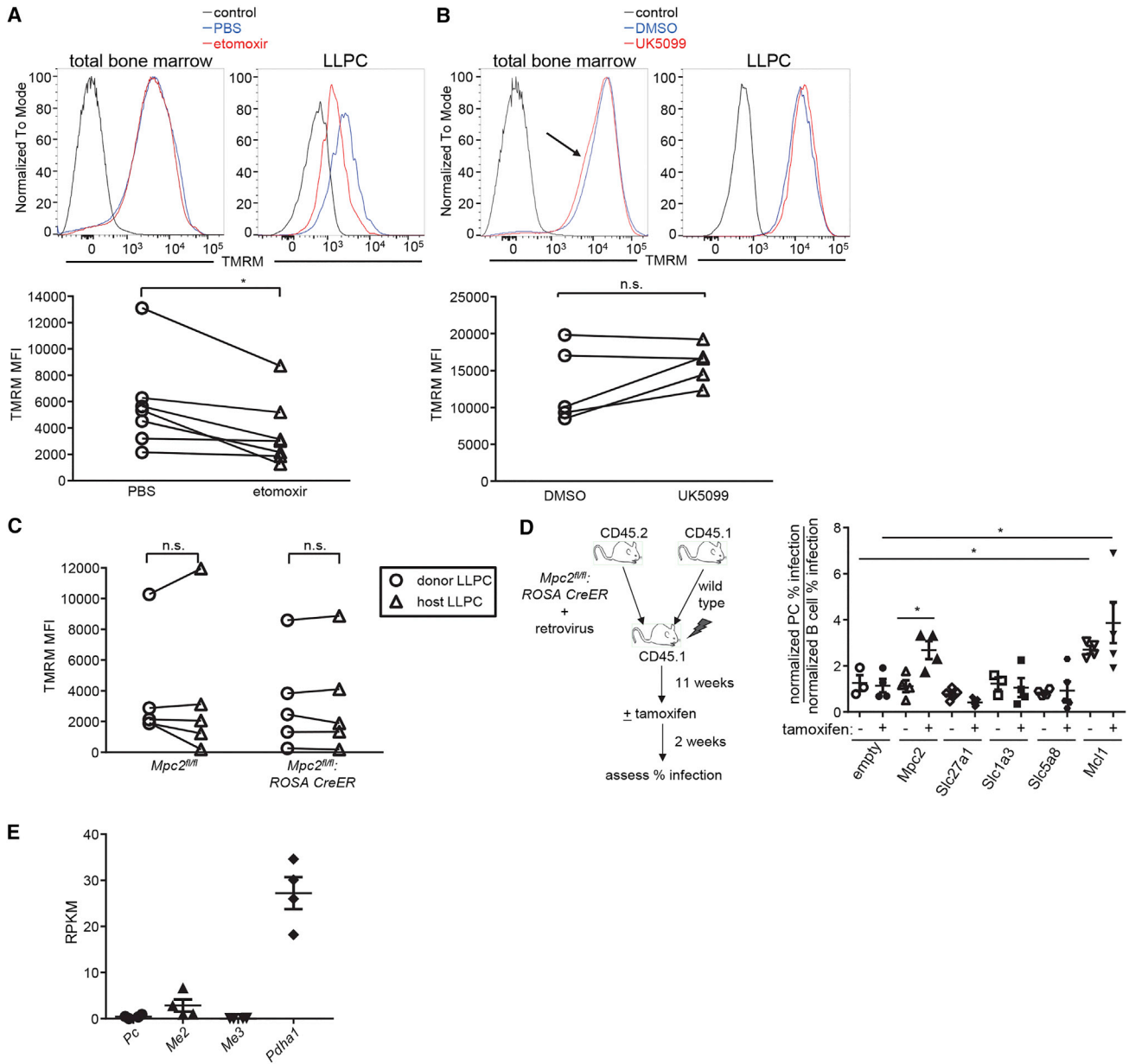


Figure 3. LCFAs Are Used for Basal Respiration In Vivo

(A) TMRM fluorescence of bone marrow plasma cells after pretreatment with etomoxir. Wild-type mice were intravenously injected with 2.5 mg etomoxir or carrier, and 1 hr later intravenously injected with 10 μ g TMRM. Animals were sacrificed 15 min later and bone marrow plasma cells were analyzed by flow cytometry. Example plots are shown, representative of seven biologically distinct samples in each treatment group. Data are quantified in bottom panel in which samples were matched for identical overall TMRM loading. * $p < 0.05$ by Student's two-tailed paired t test.

(B) TMRM fluorescence of bone marrow plasma cells after pretreatment with UK5099. Wild-type mice were intraperitoneally injected with 500 μ g UK5099 or carrier, and 1 hr later intravenously injected with 10 μ g TMRM. Animals were sacrificed 15 min later and bone marrow plasma cells were analyzed by flow cytometry. Example plots are shown, with the arrow depicting an area of reduced fluorescence observed in every UK5099 sample. Data are representative of five biologically distinct samples in each treatment group. n.s. = not significant by Student's two-tailed paired t test.

(C) TMRM staining of donor and residual host bone marrow plasma cells from *Mpc2^{fl/fl}* or *Mpc2^{fl/fl}; ROSA26-CreER* and μ MT mixed bone marrow chimeras. Chimeras were given five daily injections of tamoxifen, and administered 10 μ g intravenous TMRM 3 days after the final tamoxifen injection. Mean fluorescence intensity values (MFI) were compared between donor and host cells in the same animal. n.s. = not significant by Student's two-tailed paired t test.

(D) Retroviral bone marrow chimera analysis of *Mpc2*-deficient plasma cells. Schematic representation of experiment is shown in the left panel, and quantification of normalized survival advantage of transduced plasma cells relative to upstream B cells is shown in the right panel (see formula in Supplemental Information). * $p < 0.05$ by Student's two-tailed t test. Mean values + SEM are shown.

(E) RNA-seq analysis of mitochondrial pyruvate metabolizing enzymes in human LLPC. RPKM: reads per kilobase per million mapped reads. Mean values \pm SEM are shown. See also Figure S3.

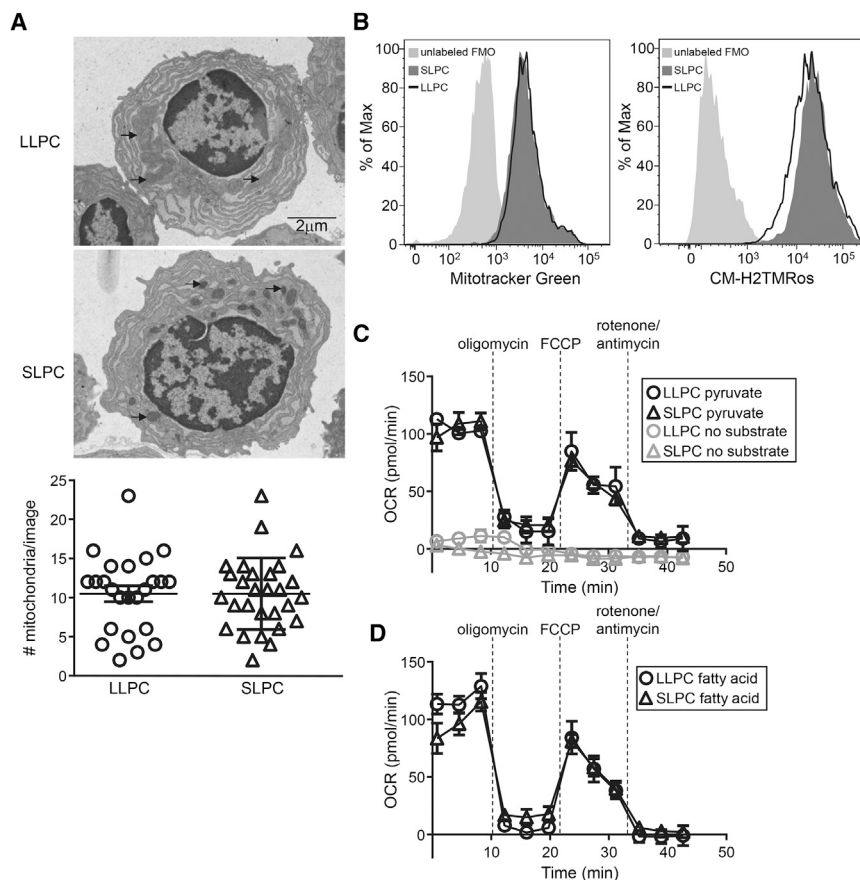


Figure 4. Mitochondrion from LLPCs and SLPCs Are Functionally Similar

(A) Representative electron micrographs of mouse LLPC (top panel) and SLPC from immunized mice (bottom panel). Arrows indicate mitochondria. Images are representative of > 60 images acquired in two separate experiments. The bottom panel shows the number of distinct mitochondria observed per image. Data were obtained from 30 images of each cell type randomly chosen from two independent experiments. Mean values + SEM are shown.

(B) Mitotracker Green (left panel) and CM-TMRos (right panel) staining of mitochondria from mouse LLPC and SLPC from immunized mice. Plots are representative of six individual experiments. FMO: fluorescence minus one control (Tung et al., 2004).

(C) OCR of permeabilized mouse LLPC and SLPC from immunized mice with or without the addition of 10 mM sodium pyruvate. Mean values of technical replicates \pm SEM are shown. Plots are representative of four independent experiments.

(D) OCR of permeabilized mouse LLPC and SLPC from immunized mice in the presence of 40 μ M palmitoyl carnitine. Mean values of technical replicates \pm SEM are shown. Plots are representative of four independent experiments.

of LCFAs (Figures S3B and S3C). Slc27a1 expression protected neutrophils from Mpc2 deficiency (Figures S3D and S3E), but failed to rescue plasma cells (Figure 3D). These data suggest that mitochondrial pyruvate and LCFAs play distinct roles in plasma cells in vivo.

LCFAs cannot be used for anaplerotic reactions to replace tricarboxylic acid cycle intermediates in mammals (Lehninger et al., 2013). Thus, mitochondrial pyruvate might be essential for anaplerosis and cataplerosis in LLPCs. For example, proliferating cells are rescued from pyruvate- and respiration-deficiency by providing aspartate through the expression of the amino acid transporter solute carrier 1a3 (Slc1a3) (Birsoy et al., 2015; Kanai and Hediger, 1992). Consistent with their requirement for glutamate and aspartate (Curi et al., 1997), expression of Slc1a3 provided an advantage to neutrophils irrespective of Mpc2 expression (Figure S3F). However, Slc1a3 expression failed to protect plasma cells in vivo (Figure 3D). Expression of solute carrier 5a8 (Slc5a8), which promotes uptake of short-chain fatty acids such as anaplerotic propionate (Miyauchi et al., 2004), also failed to rescue Mpc2 deficiency (Figure 3D). Finally, RNA-seq analysis of LLPCs revealed no transcriptional expression of pyruvate carboxylase (*Pc*), the major enzyme that catalyzes pyruvate-mediated anaplerosis (Figure 3E). In contrast, we observed high transcriptional expression of pyruvate dehydrogenase (*Pdha1*, Figure 3E), which catalyzes formation of acetyl CoA. We observed low transcriptional expression of malic enzyme 2 (*Me2*) (Figure 3E), but in vivo this enzyme preferentially

decarboxylates malate to form pyruvate rather than the reverse reaction (Zelle et al., 2011). Thus, we reasoned that pyruvate plays a non-redundant role with LCFAs not necessarily because of the unique anaplerotic reactions it can mediate, but potentially due to different metabolic cues that regulate its formation and oxidation. This could allow cells to respond more broadly to metabolic changes than would fatty acid metabolism alone.

Mitochondrion Function Similarly in SLPCs and LLPCs

We next wanted to understand how pyruvate formation and subsequent respiration were regulated in plasma cells. Increased mitochondrial mass could lead to an elevated maximal capacity to take up respiratory substrates. Through examination of electron microscopic images, we observed some morphological changes but no differences in the numbers of distinct mitochondrion between LLPCs and SLPCs (Figure 4A). Mitotracker Green and CM-H2TMRos dyes, which stain total and respiring mitochondrion, respectively, revealed no differences between LLPCs and SLPCs (Figure 4B). Next, LLPCs and SLPCs were permeabilized, thus allowing the direct delivery of substrates to the mitochondria without having to pass through cell surface transporters (Salabei et al., 2014). Under these conditions, LLPCs and SLPCs oxidized pyruvate equivalently (Figure 4C). No oxygen consumption was observed when pyruvate was omitted (Figure 4C), and pyruvate had no effect on respiration unless cells were permeabilized (data not shown). Similar results were observed when permeabilized LLPCs and SLPCs were provided palmitoyl carnitine, a LCFA (Figure 4D). These data suggest that the increased maximal respiratory capacity in LLPCs was not driven by unique cell-intrinsic mitochondrial

properties, but by respiratory substrates such as pyruvate which were less available to SLPCs.

LLPCs Constitutively Take Up Glucose

Pyruvate can be provided by multiple different metabolic pathways, including glycolysis, amino acid catabolism, and direct uptake from extracellular sources (Halestrap, 2012). We treated mouse LLPCs with sodium iodoacetate, an inhibitor of glyceraldehyde-3-phosphate dehydrogenase (GAPDH). GAPDH enzymatic activity is essential for pyruvate generation from glycolysis, but not other pathways. After iodoacetate treatment, maximal respiratory capacity in LLPCs was specifically attenuated (Figure 5A). Reduction of glucose in the media also led to a loss of maximal respiratory capacity (Figure 5B). Thus glycolysis is likely the major source of mitochondrial pyruvate in LLPCs.

We reasoned that there were two possible mechanisms by which glucose specifically mediated the increase in respiration following FCCP treatment. First, glucose could be taken up only after FCCP treatment. Second, glucose could be constitutively taken up by LLPCs for other metabolic pathways, but then diverted to pyruvate production for respiration after FCCP. To distinguish between these alternatives, we measured *in vitro* uptake of a metabolizable fluorescent glucose analog, 2NBDG (Yoshioka et al., 1996), with and without FCCP. Without FCCP, mouse LLPCs displayed more 2NBDG fluorescence than did SLPCs, indicating enhanced glucose import, potentially due to elevated expression of the glucose transporter GLUT1 (Figure S4A). Both LLPCs and SLPCs displayed less 2NBDG fluorescence and expressed less cell surface GLUT1 after treatment with FCCP (Figure S4A). Treatment of cells with 2,4-DNP, a different uncoupling agent, led to a similar degree of respiration as did treatment with FCCP (Figure S4B). These data demonstrated that LLPCs took up more glucose than SLPCs *in vitro*, and that this uptake was not enhanced by mitochondrial uncoupling.

To confirm these findings *in vivo*, we intravenously injected 2NBDG into mice that had been immunized with NP-CGG 7 days earlier. Mice were sacrificed 15 min after injection, and 2NBDG uptake in bone marrow and splenic plasma cells was measured. Approximately 80% of bone marrow plasma cells were 2NBDG^{high} (Figure 5C). In contrast, only half of splenic plasma cells were 2NBDG^{high} (Figure 5C). Because not all splenic plasma cells are necessarily short-lived (Sze et al., 2000), we examined the 2NBDG^{high} frequency in antigen-specific NP-binding splenic plasma cells. At Day 7 post-immunization, the majority of these cells are short-lived (Smith et al., 1994; Sze et al., 2000). Within this mostly short-lived NP-specific compartment, only ~20% of cells had taken up 2NBDG (Figure 5C). At 6 weeks post-immunization, by which point most LLPCs have been formed and SLPCs diminish (Han et al., 1995; Weisel et al., 2016), the majority of NP-specific bone marrow plasma cells were 2NBDG^{high} (Figure 5D). Given that we were unable to identify NP-specific SLPCs within the splenic 2NBDG^{high} compartment (Figures 5C and 5D), it seems likely that these cells represent long-lived splenic plasma cells that have been shown to exist by others (Sze et al., 2000). Moreover, these data suggest that the differences we observed in glucose import were hallmark features of LLPCs versus SLPCs rather than traits imposed by distinct anatomical sites.

We next considered the possibility that plasma cell glucose uptake was a function of proliferation rather than longevity. In unimmunized mice, a subset of the splenic B220⁺ CD138⁺ compartment is proliferative, whereas the B220⁺ CD138⁺ population is quiescent (Figure 5E, (Chernova et al., 2014; Kallies et al., 2004)). Within both the proliferative B220⁺ and quiescent B220⁺ plasma cell compartments, approximately half the populations were 2NBDG^{high} (Figure 5F). 2NBDG^{high} splenic plasma cells displayed similar respiration as did bone marrow plasma cells under both high and physiological glucose and amino acid concentrations (Figures 5G, S4C, Table S1). In contrast, 2NBDG^{low} splenic plasma cells showed limited maximal respiratory capacity in high glucose media and were unable to increase respiration after FCCP treatment at physiological glucose levels (Figures 5G and S4C). 2NBDG^{low} cells also exhibited a reduced basal respiration rate relative to their 2NBDG^{high} counterparts under physiological glucose and amino acid conditions (Figure S4C), but this difference was unaffected by UK5099 and therefore not mediated by pyruvate (Figure S4D). These data demonstrate that mouse LLPCs constitutively take up more glucose *in vivo* than do SLPCs irrespective of proliferative status.

LLPCs Use Glucose to Glycosylate Antibodies but Can Induce Glycolysis

Glucose is constitutively taken up by LLPCs, but minimally used for respiration in short time periods. Using intracellular staining (Baba, 1993), we observed that glycogen levels were actually higher in SLPCs than in LLPCs (Figure 6A). These data suggest that glucose taken up by LLPCs is used for pathways other than glycogen synthesis.

To identify metabolic fates of glucose, we sought to perform tracing experiments. Given the paucity of mouse LLPCs, we first confirmed that human LLPCs also used glucose for maximal respiratory capacity (Figure 6B) and displayed higher 2NBDG fluorescence than did SLPCs after *in vitro* culture (Figure 6C). Human LLPCs were then cultured in ¹³C glucose media. Mass spectrometry demonstrated that cells imported ¹³C glucose and converted it to glucose-6-phosphate (Figure 6D). Yet we observed very little ¹³C enrichment in pyruvate (Figure 6D). We observed comparably low ¹³C enrichment in lactate, and no enrichment in aspartate or stearate (Figure S5). UK5099 treatment diminished ¹³C enrichment in citrate (Figure 6D), confirming that the small amount of pyruvate generated under these conditions could be transported into the mitochondria. These citrate isotopomers were labeled at 2, but not 3 atoms with ¹³C, and thus were likely derived via pyruvate dehydrogenase and acetyl coA (Figure 6D). We observed substantial ¹³C enrichment in mannose (Figure 6D), which is trimmed from glycoproteins by endoplasmic reticulum-resident mannosidases (Kornfeld and Kornfeld, 1985). ¹³C-enriched mannose suggests that glucose is used for glycosylation of secreted proteins, most of which are antibodies in LLPCs (Hibi and Dosch, 1986; Shi et al., 2015).

We next cultured human LLPCs with ¹⁴C glucose to quantify the proportion that is used for antibody glycosylation. Antibodies were immunoprecipitated, treated with PNGase F to remove glycosylation, and ¹⁴C counts were measured. Remarkably, ~90% of cellular glucose was used for antibody glycosylation (Figure 7A). Glycosylation is essential for proper antibody secretion (Hickman et al., 1977). Thus, we reasoned that 2NBDG^{low}

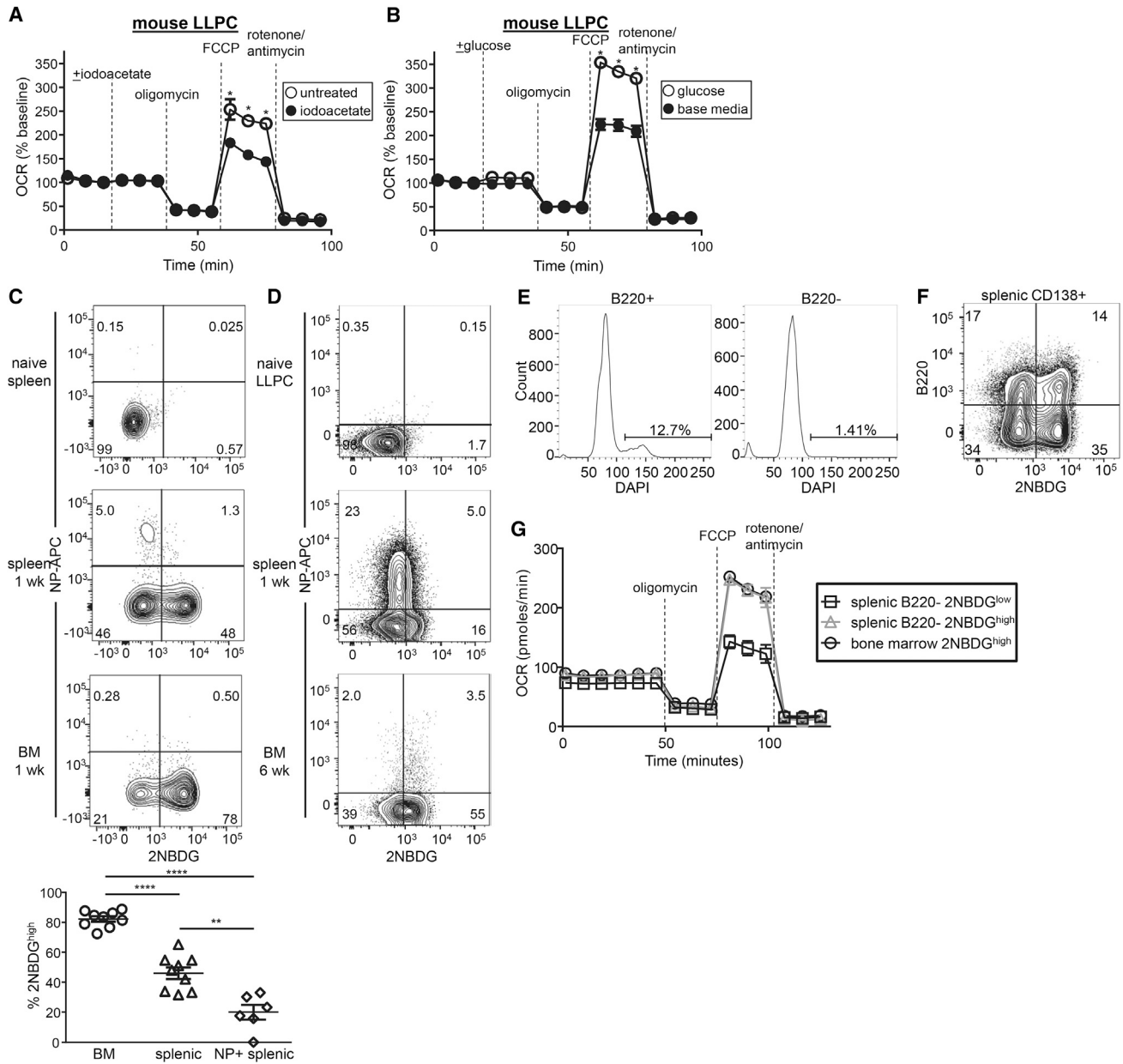


Figure 5. Mouse LLCs Take Up More Glucose Than Do SLPCs

(A) OCR of mouse LLC after inhibition of glycerolaldehyde 3-phosphate dehydrogenase. LLCs were left untreated or treated with 50 μ M iodoacetate, and OCR was measured. Plot is representative of three independent experiments. Mean values of technical replicates \pm SEM are shown. OCR values are normalized to the reading just prior to the injection of iodoacetate. * $p < 0.05$, by Student's two-tailed t test.

(B) OCR of mouse LLC after reduction of extracellular glucose. LLCs were in base 11 mM glucose media. OCR was measured with and without injection of glucose to a final concentration of 25 mM. Plot is representative of three independent experiments. Mean values of technical replicates \pm SEM are shown. OCR values are normalized to the reading just prior to the injection of glucose. * $p < 0.05$, by Student's two-tailed t test.

(C) Flow cytometric quantification of 2NBDG uptake in vivo by LLC and SLPC. 2NBDG (100 μ g) was injected intravenously into mice and spleens and BM were harvested 15 min later. Top panel represents splenic plasma cells from an unimmunized mouse that was not injected with 2NBDG. Middle and bottom panels are from a 2NBDG-injected mouse immunized 7 days prior with NP-CGG. Quantification of 2NBDG^{high} cells across biologically distinct samples are shown in the bottom panel. Mean values \pm SEM are shown. Data are cumulative from three independent experiments. **** $p < 0.00005$, ** $p < 0.005$ by one-way ANOVA.

(D) Flow cytometric quantification of 2NBDG uptake in vivo by antigen-specific LLC and SLPC. 2NBDG (100 μ g) was injected intravenously into mice and spleens and BM were harvested 15 min later. NP-specific plasma cells were detected through a modified antibody capture assay (see [Supplemental Experimental Procedures](#)). Top panel represents bone marrow plasma cells from an unimmunized mouse that was not injected with 2NBDG. Middle panel is from a 2NBDG-injected mouse immunized 7 days prior with NP-CGG, and bottom panel is from a mouse immunized with NP-CGG 6 weeks earlier. Data are representative of two independent experiments.

(E) Cell cycle analysis of B220⁺ or B220⁻ splenic plasma cells from an unimmunized mouse. Data are representative of two independent experiments.

(legend continued on next page)

SLPCs, which take up much less glucose than do LLPCs (Figures 5C-D), would also secrete fewer antibodies. Indeed, 2NBDG^{low} plasma cells secreted ~5-fold fewer antibodies than did their 2NBDG^{high} counterparts under physiological glucose and amino acid concentrations (Figure 7B).

The metabolic decision point between glycolysis and hexosamine biosynthesis for glycosylation occurs at fructose-6-phosphate, catalyzed by phosphofruktokinase (PFK) and glutamine-fructose-6-phosphate transaminase (GFPT1), respectively. We hypothesized that regulators that activate PFK activity, such as lowered ATP levels, would lead to the formation of pyruvate. Treatment of cells with oligomycin led to an increase in extracellular acidification rates (ECAR) through lactate excretion (Figure 7C). Similarly, inhibiting the oxidation of alternate respiratory substrates such as long-chain fatty acids with etomoxir led to an increase in lactate (Figure 7C). ECAR was inhibited by iodoacetate (Figure 7C), demonstrating dependence on glycolysis and pyruvate production. Under physiological glucose conditions, LLPCs but not SLPCs were able to generate lactate after oligomycin or FCCP treatment (Figure S4C). We reasoned that stimuli which divert glucose to glycolysis and pyruvate for respiration would reduce antibody secretion, in part by limiting glycosylation. Overnight oligomycin treatment reduced LLPC viability (data not shown), but FCCP led to a marked decrease in antibody secretion (Figure 7C), without affecting survival (data not shown). Part of this effect might be indirect and caused by mitochondrial dysfunction. Yet taking together the experiments in Figure 7, the data indicate that LLPCs predominantly use glucose to glycosylate antibodies, but also use glycolysis and pyruvate-dependent respiration under metabolic conditions that activate PFK. By virtue of their inability to take up as much glucose, SLPCs are less able to engage these pathways.

DISCUSSION

Durable antibody-mediated immunity to infections is mediated by LLPCs, and the majority of vaccines used clinically depend upon the production of neutralizing antibodies to confer protection (Amanna and Slifka, 2011). Yet very little is known regarding features of the immunogen or host genetic factors that confer durable antibody responses. Thus, a better fundamental understanding of the mechanisms behind LLPC persistence is needed. Here, we have demonstrated that SLPCs and LLPCs are functionally distinguished by pyruvate-dependent mitochondrial respiratory capacity *in vivo*.

We observed that LLPCs imported more glucose constitutively *in vivo* than did SLPCs. Stimuli such as low ATP levels activated PFK, thus diverting glucose to glycolysis and pyruvate formation for respiration in LLPCs. Why this essential function could not be performed by LCFAs is unclear. One explanation is that the regulation of pyruvate formation and oxidation are not subject to the same controls as fatty acid oxidation. For example, malonyl coA is a major negative regulator of fatty acid oxidation (McGarry et al., 1977), whereas ATP directly inhibits PFK (Garland et al.,

1963). By this logic, LLPCs have the ability to enact different metabolic switches in response to distinct changes in the environment. What are these changes? It is likely that pyruvate is made by LLPCs and used for respiration under normal conditions as an essential response to numerous perturbations that occur frequently. For example, serum glucose and free fatty acid concentrations vary substantially over the course of a day for many reasons including meals, circadian rhythms, etc. (Schlierf and Dorow, 1973). Mitochondrial pyruvate import in LLPCs thus buffers against these changes to maintain energy homeostasis and durable humoral immunity.

Through the course of these studies, we discovered substantial heterogeneity within both bone marrow and splenic plasma cells in the ability to import a fluorescent glucose analog. Within the B220⁻ subsets of these populations, 2NBDG import correlated well with plasma cell longevity. Short-lived antigen specific plasma cells formed early after immunization were 2NBDG^{low}, whereas long-lived antigen-specific plasma cells formed late in the response were mostly 2NBDG^{high}. Yet the functional significance of 2NBDG import in the B220⁺ plasma cell subset, which turns over rapidly (Chernova et al., 2014), is unknown. The data imply that although glucose import and mitochondrial pyruvate import are necessary for long-term plasma cell survival, they might not be sufficient to prolong lifespan. Alternatively, the 2NBDG^{high} subset of B220⁺ plasma cells might in fact be self-renewing and long-lived as a population (Tooze, 2013).

Here we have shown that glucose import, pyruvate transport, and spare respiratory capacity are necessary for plasma cell longevity. An open question is which physiological signals promote these metabolic properties. The cell surface expression of Glut1 is higher in LLPCs than in SLPCs despite similar transcription. This implies the existence of LLPC-specific signals that promote Glut1 and/or other glucose transporter expression and activity post-transcriptionally. Knowledge of these signals could instruct rational vaccine design to enhance the durability of protection against infectious disease.

EXPERIMENTAL PROCEDURES

Detailed experimental procedures can be found in the [Supplemental Information](#).

Mice

All procedures in this study were approved by the Institutional Animal Care and Use Committee at Washington University. C57Bl6/N mice were housed and bred in pathogen-free facilities. B6.Ly5.2 (CD45.1) mice used in chimera experiments were obtained from the National Cancer Institute, and C57BL/6J-IgH^g mice were obtained from The Jackson Laboratory. *Mpc2^{fl/fl}* mice were generated as recently described (McCommis et al., 2015). These mice were crossed to ROSA26-CreER mice obtained from The Jackson Laboratory.

Human Tissues

Tonsils were obtained from children undergoing elective tonsillectomy (St. Louis Children's Hospital). Bone marrow was obtained from total hip arthroplasty samples from patients undergoing elective surgery (Barnes Jewish Hospital). All samples were kept anonymous with no identifying information. All

(F) Flow cytometric quantification of 2NBDG uptake *in vivo* by splenic plasma cells from an unimmunized mouse. Data are representative of eight independent experiments.

(G) OCR of 2NBDG⁺ or 2NBDG⁻ splenic and bone marrow plasma cells from unimmunized mice. Data are representative of four independent experiments. Mean values of technical triplicates + SEM are shown. See also Figure S4.

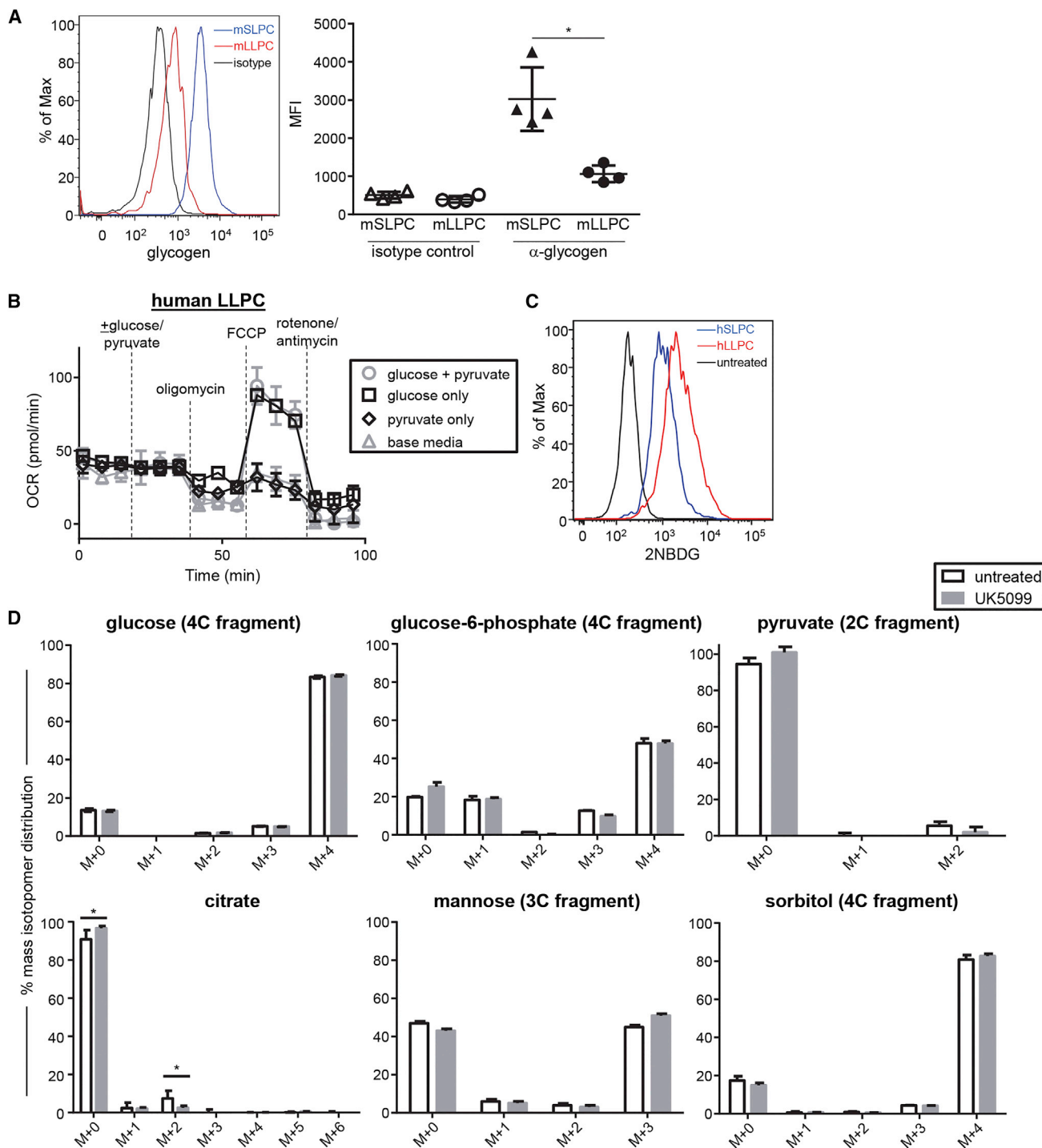


Figure 6. LLPCs Catabolize Glucose for Protein Glycosylation under Basal Conditions

(A) LLPC (red lines) or SLPC from immunized mice (blue lines) were intracellularly stained with α -glycogen monoclonal antibody or an isotype control. MFI values \pm SEM are shown in the right panel. Data are representative of two independent experiments.

(B) OCR of human LLPC after exclusion of extracellular glucose. OCR was measured with and without injection of glucose to a final concentration of 25 mM and/or pyruvate to a final concentration of 1 mM. Plot is representative of three independent experiments. Mean values of technical replicates \pm SEM are shown.

(C) Flow cytometric analysis of in vitro 2NBDG uptake in human LLPC (red line) and SLPC (blue line). Plot is representative of three independent experiments using biologically distinct samples.

(legend continued on next page)

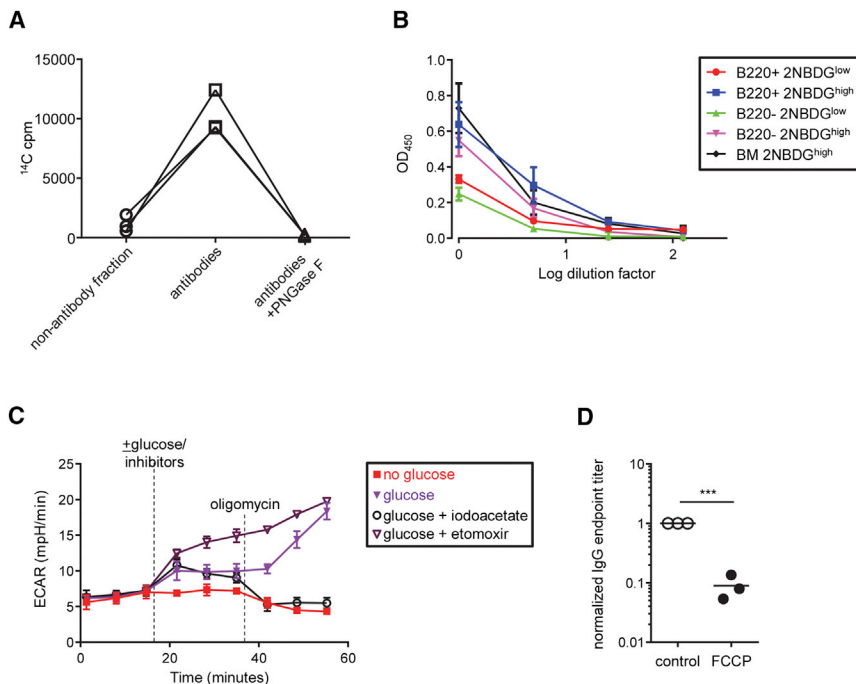


Figure 7. Antibody Glycosylation Consumes the Majority of Cellular Glucose in LLCs

(A) ¹⁴C-tracing of glucose carbons in antibodies and glycosylation sugars. Human LLCs were cultured overnight in the presence of ¹⁴C glucose, and antibodies from the supernatant and cell lysate were immunoprecipitated. Radioactive counts in the cellular non-antibody fraction and immunoprecipitated antibodies left untreated or treated with the deglycosylation enzyme PNGase F are shown. Each data point represents a biologically distinct sample.

(B) Measurement of antibody secretion by mouse plasma cells. 10,000 polyclonal splenic and bone marrow plasma cell subsets from unimmunized mice as indicated were cultured for 16 hr in 5% O₂ and media containing 9 mM glucose and physiological concentrations of amino acids (see Table S1). Total secreted IgG antibodies were quantified by ELISA. Data include three biological replicates for each cell type. Mean values ± SEM are shown.

(C) Measurement of extracellular acidification rates of mouse LLC after addition of glucose ± iodoacetate or etomoxir and oligomycin. Mean values of technical triplicates ± SEM are shown.

(D) Quantification of antibody production in human LLC treated with FCCP. Human LLCs were cultured overnight in the presence or absence of FCCP. Antibody concentrations in the supernatant were measured by ELISA. Data are normalized to the untreated sample. ***p < 0.0001 by Student's ratio t test.

procedures in this study were approved by the Human Research Protection Office at Washington University.

Flow Cytometry and Microscopy

For in vitro experiments, dyes were used as follows: Mitotracker Green FM (50 nM), Mitotracker Orange CMH2TMRos (100 nM), and 2NBDG (50 μg/ml). For in vivo 2NBDG stains, mice were injected retro-orbitally with 100 μg 2NBDG in PBS. For in vivo TMRM experiments, mice were treated with 2.5 mg etomoxir intravenously (i.v.) or 500 μg UK5099 intraperitoneally (i.p.) before being injected with 10 μg TMRM i.v. For glycogen stains, cells were fixed, permeabilized, and stained with 1 μg α-glycogen monoclonal antibody. For cell cycle analysis, cells were fixed, permeabilized, and incubated with 10 μg/ml DAPI. For transmission, EM cells were sorted and fixed in 2% paraformaldehyde /2.5% glutaraldehyde in 100mM cacodylate buffer pH 7.2. Sections were stained with uranyl acetate and lead citrate.

Extracellular Flux Assays

All extracellular flux assays were performed with Seahorse Bioscience XF96 Analyzers. Inhibitors were added at the following final concentrations: UK5099 (10 μM), etomoxir (20 μM), DON (50 μM), sodium iodoacetate (50 μM), oligomycin (1 μM), FCCP (1.5 μM), Rotenone (100nM), Antimycin A (1 μM), aminooxyacetic acid (500 μM). For permeabilization, cells were treated with 1nM perfringolysin O + 4 mM ADP + 0.5 mM malate in the presence or absence of 10 mM pyruvate or 40 μM palmitoyl carnitine (Salabei et al., 2014).

RNA Sequencing

Libraries were made and single end 50 bp reads were acquired using an Illumina HiSeq 2500. Reads were mapped to the Ensembl_R72 reference human

genome using Tophat. RNA-seq data can be downloaded with GEO accession GSE81443.

DNA Constructs and Retroviral Production

Constructs were cloned into the murine stem cell virus (MSCV)-IRES-GFP or MSCV-IRES-Thy1.1 vectors. Lenti-X 293T cells were cultured and transfected using 30 μl FuGene HD with 1.75 μg pMD2.G, 3.25 μg of pBS CMV-gag-pol, and 5 μg of retroviral vector.

Bone Marrow Chimeras

For competitive reconstitutions, 5 × 10⁶ bone marrow cells from either *Mpc2^{fl/fl}* or *Mpc2^{fl/fl};ROSA26 CreER* littermates were mixed with 5 × 10⁶ bone marrow cells from either B6.Ly5.2 CD45.1⁺ mice or C57BL/6J-IgH^a mice and transferred into 800 cGy-irradiated B6.Ly5.2 CD45.1⁺ IgH^a recipients. At the indicated times, animals were injected i.p. for 5 consecutive days with 50 μg of tamoxifen dissolved in corn oil per gram of mouse weight. For retroviral chimeras, bone marrow was enriched for c-kit⁺ cells using CD117⁺ microbeads. 50,000 to 100,000 cells were cultured overnight and five μl of polyethylene glycol-concentrated virus was added to the cultures the following day. Cells were washed, mixed, and transferred as described above.

WNV Vaccination and ELISA

Chimeras were immunized i.p. with 100 μl West Nile Virus Innovator vaccine (Fort Dodge) for two consecutive days. ELISA plates were coated with 5 μg/ml WNV domain III protein. Serum was probed with 1 μg/ml biotinylated anti-mouse IgG2a^a or anti-IgG2a^b. OD were measured at 450 nm.

(D) Gas chromatographic-mass spectrometric analysis of ¹³C enrichment in human LLC metabolites. Human LLC metabolites 18 hr after culture with ¹³C-glucose-containing media with (shaded bars) or without (empty bars) UK5099. Distributions of isotopomers are shown with background correction using matched ¹²C-glucose cultures. M+0 peaks represent fragments in which every carbon has an atomic mass of 12. The total number of carbon atoms in the analyzed fragment is shown for each metabolite. Mean values of biological replicates ± SEM are shown; n = 8 for untreated samples, n = 5 for UK5099-treated samples. *p < 0.05 by Student's two-tailed t test. See also Figure S5.

B Cell Cultures

For *in vitro* antibody secretion assays, 10^4 plasma cells were plated per well and cultured overnight. Antibodies in the supernatant were captured on α -Ig κ -coated ELISA plates, and detected with IgH-specific antibodies.

^{13}C and ^{14}C Tracing Experiments

Human samples were cultured with ^{13}C - or $2\mu\text{M}$ ^{14}C glucose overnight. For ^{14}C experiments, antibodies were isolated with protein G beads and treated with PNGase F.

ACCESSION NUMBERS

The accession number for RNA-seq data reported in this paper is NCBI GEO:GSE81443.

SUPPLEMENTAL INFORMATION

Supplemental Information includes five figures, one table, and Supplemental Experimental Procedures and can be found with this article online at <http://dx.doi.org/10.1016/j.immuni.2016.06.011>.

AUTHOR CONTRIBUTIONS

D.B., E.L.P., G.J.P., M.J.W., and B.N.F. designed the study. A.M.B., K.M.K., R.W., W.Y.L., J.D.C., K.S.M., J.F., H.A.P., R.N., E.M.L., J.L., and D.B. performed experiments. A.M.B., K.M.K., R.W., W.Y.L., J.D.C., K.S.M., J.F., R.N., G.J.P., E.M.L., B.N.F., E.L.P., and D.B. analyzed the data. D.B. wrote the paper, and all other authors edited the paper.

ACKNOWLEDGMENTS

This work was supported by NIH grants R01AI099108 (D.B.), R01AI091965 (E.L.P.), R01DK104735 (B.N.F.), R42AA021228 (B.N.F.), R01NS072241 (M.J.W.), and K01DK099395 (A.M.B.). This work was also supported by the New York Stem Cell Foundation and a Research Scholar grant from the American Cancer Society (125091-RSG-13-252-01-LIB, to D.B.). D.B. is a New York Stem Cell Foundation-Robertson Investigator. K.S.M. is a Diabetes Research Postdoctoral Training Program fellow (T32 DK07296 and DK007120). R.W. is supported by a predoctoral fellowship from the National Science Foundation (DGE-1143954). The West Coast Metabolomics Center is supported by NIH grant U24 DK-097154. RNA-seq analysis was performed by the Genome Technology Access Center at Washington University, supported by NIH grants P30CA91842 (Sitman Cancer Center) and UL1TR000448 (ICTS/CTSA). G.J.P. is a scientific advisory board member for Cambridge Isotope Laboratories. R.M.N. is a paid consultant for Bio-composites, Cardinal Health; CardioMEMS; DePuy, A Johnson & Johnson Company; Integra Sciences; Medtronic; Smith & Nephew; and Wright Medical Technology, Inc.

Received: August 14, 2015

Revised: February 19, 2016

Accepted: April 9, 2016

Published: July 5, 2016

REFERENCES

- Ahuja, A., Anderson, S.M., Khalil, A., and Shlomchik, M.J. (2008). Maintenance of the plasma cell pool is independent of memory B cells. *Proc. Natl. Acad. Sci. USA* *105*, 4802–4807.
- Amanna, I.J., and Slifka, M.K. (2011). Contributions of humoral and cellular immunity to vaccine-induced protection in humans. *Virology* *411*, 206–215.
- Amanna, I.J., Carlson, N.E., and Slifka, M.K. (2007). Duration of humoral immunity to common viral and vaccine antigens. *N. Engl. J. Med.* *357*, 1903–1915.
- Baba, O. (1993). [Production of monoclonal antibody that recognizes glycogen and its application for immunohistochemistry]. *Kokubyo Gakkai zasshi. The Journal of the Stomatological Society, Japan* *60*, 264–287.
- Benner, R., Hijmans, W., and Haaijman, J.J. (1981). The bone marrow: the major source of serum immunoglobulins, but still a neglected site of antibody formation. *Clin. Exp. Immunol.* *46*, 1–8.
- Berek, C., Berger, A., and Apel, M. (1991). Maturation of the immune response in germinal centers. *Cell* *67*, 1121–1129.
- Birsoy, K., Wang, T., Chen, W.W., Freinkman, E., Abu-Remaileh, M., and Sabatini, D.M. (2015). An Essential Role of the Mitochondrial Electron Transport Chain in Cell Proliferation Is to Enable Aspartate Synthesis. *Cell* *162*, 540–551.
- Bricker, D.K., Taylor, E.B., Schell, J.C., Orsak, T., Boutron, A., Chen, Y.C., Cox, J.E., Cardon, C.M., Van Vranken, J.G., Dephoure, N., et al. (2012). A mitochondrial pyruvate carrier required for pyruvate uptake in yeast, *Drosophila*, and humans. *Science* *337*, 96–100.
- Cambridge, G., Leandro, M.J., Edwards, J.C., Ehrenstein, M.R., Salden, M., Bodman-Smith, M., and Webster, A.D. (2003). Serologic changes following B lymphocyte depletion therapy for rheumatoid arthritis. *Arthritis Rheum.* *48*, 2146–2154.
- Caro-Maldonado, A., Wang, R., Nichols, A.G., Kuraoka, M., Milasta, S., Sun, L.D., Gavin, A.L., Abel, E.D., Kelsoe, G., Green, D.R., and Rathmell, J.C. (2014). Metabolic reprogramming is required for antibody production that is suppressed in anergic but exaggerated in chronically BAFF-exposed B cells. *J. Immunol.* *192*, 3626–3636.
- Chernova, I., Jones, D.D., Wilmore, J.R., Bortnick, A., Yucel, M., Hershberg, U., and Allman, D. (2014). Lasting antibody responses are mediated by a combination of newly formed and established bone marrow plasma cells drawn from clonally distinct precursors. *J. Immunol.* *193*, 4971–4979.
- Choi, S.W., Gerencser, A.A., and Nicholls, D.G. (2009). Bioenergetic analysis of isolated cerebrocortical nerve terminals on a microgram scale: spare respiratory capacity and stochastic mitochondrial failure. *J. Neurochem.* *109*, 1179–1191.
- Curi, T.C., De Melo, M.P., De Azevedo, R.B., Zorn, T.M., and Curi, R. (1997). Glutamine utilization by rat neutrophils: presence of phosphate-dependent glutaminase. *Am. J. Physiol.* *273*, C1124–C1129.
- DiLillo, D.J., Hamaguchi, Y., Ueda, Y., Yang, K., Uchida, J., Haas, K.M., Kelsoe, G., and Tedder, T.F. (2008). Maintenance of long-lived plasma cells and serological memory despite mature and memory B cell depletion during CD20 immunotherapy in mice. *J. Immunol.* *180*, 361–371.
- Doughty, C.A., Bleiman, B.F., Wagner, D.J., Dufort, F.J., Mataraza, J.M., Roberts, M.F., and Chiles, T.C. (2006). Antigen receptor-mediated changes in glucose metabolism in B lymphocytes: role of phosphatidylinositol 3-kinase signaling in the glycolytic control of growth. *Blood* *107*, 4458–4465.
- Dufort, F.J., Bleiman, B.F., Gumina, M.R., Blair, D., Wagner, D.J., Roberts, M.F., Abu-Amer, Y., and Chiles, T.C. (2007). Cutting edge: IL-4-mediated protection of primary B lymphocytes from apoptosis via Stat6-dependent regulation of glycolytic metabolism. *J. Immunol.* *179*, 4953–4957.
- Dufort, F.J., Gumina, M.R., Ta, N.L., Tao, Y., Heyse, S.A., Scott, D.A., Richardson, A.D., Seyfried, T.N., and Chiles, T.C. (2014). Glucose-dependent de novo lipogenesis in B lymphocytes: a requirement for atp-citrate lyase in lipopolysaccharide-induced differentiation. *J. Biol. Chem.* *289*, 7011–7024.
- Fagraeus, A. (1948). The plasma cellular reaction and its relation to the formation of antibodies *in vitro*. *J. Immunol.* *58*, 1–13.
- Garcia-Manteiga, J.M., Mari, S., Godejohann, M., Spraul, M., Napoli, C., Cenci, S., Musco, G., and Sitia, R. (2011). Metabolomics of B to plasma cell differentiation. *J. Proteome Res.* *10*, 4165–4176.
- Garland, P.B., Randle, P.J., and Newsholme, E.A. (1963). Citrate as an Intermediary in the Inhibition of Phosphofructokinase in Rat Heart Muscle by Fatty Acids, Ketone Bodies, Pyruvate, Diabetes, and Starvation. *Nature* *200*, 169–170.
- Halestrap, A.P. (2012). The mitochondrial pyruvate carrier: has it been unearthed at last? *Cell Metab.* *16*, 141–143.
- Hall, A.M., Rhodes, G.J., Sandoval, R.M., Corridon, P.R., and Molitoris, B.A. (2013). *In vivo* multiphoton imaging of mitochondrial structure and function during acute kidney injury. *Kidney Int.* *83*, 72–83.

- Han, S., Hathcock, K., Zheng, B., Kepler, T.B., Hodes, R., and Kelsoe, G. (1995). Cellular interaction in germinal centers. Roles of CD40 ligand and B7-2 in established germinal centers. *J. Immunol.* *155*, 556–567.
- Herzig, S., Raemy, E., Montessuit, S., Veuthey, J.L., Zamboni, N., Westermann, B., Kunji, E.R., and Martinou, J.C. (2012). Identification and functional expression of the mitochondrial pyruvate carrier. *Science* *337*, 93–96.
- Hibi, T., and Dosch, H.M. (1986). Limiting dilution analysis of the B cell compartment in human bone marrow. *Eur. J. Immunol.* *16*, 139–145.
- Hickman, S., Kulczycki, A., Jr., Lynch, R.G., and Kornfeld, S. (1977). Studies of the mechanism of tunicamycin in inhibition of IgA and IgE secretion by plasma cells. *J. Biol. Chem.* *252*, 4402–4408.
- Jacob, J., Kassir, R., and Kelsoe, G. (1991). In situ studies of the primary immune response to (4-hydroxy-3-nitrophenyl)acetyl. I. The architecture and dynamics of responding cell populations. *J. Exp. Med.* *173*, 1165–1175.
- Jang, K.J., Mano, H., Aoki, K., Hayashi, T., Muto, A., Nambu, Y., Takahashi, K., Itoh, K., Taketani, S., Nutt, S.L., et al. (2015). Mitochondrial function provides instructive signals for activation-induced B-cell fates. *Nat. Commun.* *6*, 6750.
- Kallies, A., Hasbold, J., Tarlinton, D.M., Dietrich, W., Corcoran, L.M., Hodgkin, P.D., and Nutt, S.L. (2004). Plasma cell ontogeny defined by quantitative changes in blimp-1 expression. *J. Exp. Med.* *200*, 967–977.
- Kanai, Y., and Hediger, M.A. (1992). Primary structure and functional characterization of a high-affinity glutamate transporter. *Nature* *360*, 467–471.
- Kornfeld, R., and Kornfeld, S. (1985). Assembly of asparagine-linked oligosaccharides. *Annu. Rev. Biochem.* *54*, 631–664.
- Lee, K., Heffington, L., Jellusova, J., Nam, K.T., Raybuck, A., Cho, S.H., Thomas, J.W., Rickert, R.C., and Boothby, M. (2013). Requirement for Rictor in homeostasis and function of mature B lymphoid cells. *Blood* *122*, 2369–2379.
- Lehninger, A.L., Nelson, D.L., and Cox, M.M. (2013). *Lehninger principles of biochemistry*, Sixth Edition (New York: W.H. Freeman).
- Manz, R.A., Thiel, A., and Radbruch, A. (1997). Lifetime of plasma cells in the bone marrow. *Nature* *388*, 133–134.
- Manz, R.A., Löhning, M., Cassese, G., Thiel, A., and Radbruch, A. (1998). Survival of long-lived plasma cells is independent of antigen. *Int. Immunol.* *10*, 1703–1711.
- McCommis, K.S., Chen, Z., Fu, X., McDonald, W.G., Colca, J.R., Kletzien, R.F., Burgess, S.C., and Finck, B.N. (2015). Loss of mitochondrial pyruvate carrier 2 in liver leads to defects in gluconeogenesis and compensation via pyruvate-alanine cycling. *Cell Metab.* *22*, 682–694.
- McGarry, J.D., Mannaerts, G.P., and Foster, D.W. (1977). A possible role for malonyl-CoA in the regulation of hepatic fatty acid oxidation and ketogenesis. *J. Clin. Invest.* *60*, 265–270.
- Miyauchi, S., Gopal, E., Fei, Y.J., and Ganapathy, V. (2004). Functional identification of SLC5A8, a tumor suppressor down-regulated in colon cancer, as a Na(+)-coupled transporter for short-chain fatty acids. *J. Biol. Chem.* *279*, 13293–13296.
- O'Connor, B.P., Raman, V.S., Erickson, L.D., Cook, W.J., Weaver, L.K., Ahonen, C., Lin, L.L., Mantchev, G.T., Bram, R.J., and Noelle, R.J. (2004). BCMA is essential for the survival of long-lived bone marrow plasma cells. *J. Exp. Med.* *199*, 91–98.
- Olotu, A., Fegan, G., Wambua, J., Nyangweso, G., Awuondo, K.O., Leach, A., Lievens, M., Lebouleux, D., Njuguna, P., Peshu, N., et al. (2013). Four-year efficacy of RTS,S/AS01E and its interaction with malaria exposure. *The New England journal of medicine* *368*, 1111–1120.
- Pengo, N., Scolari, M., Oliva, L., Milan, E., Mainoldi, F., Raimondi, A., Fagioli, C., Merlini, A., Mariani, E., Pasqualetto, E., et al. (2013). Plasma cells require autophagy for sustainable immunoglobulin production. *Nat. Immunol.* *14*, 298–305.
- Peperzak, V., Vikström, I., Walker, J., Glaser, S.P., LePage, M., Coquery, C.M., Erickson, L.D., Fairfax, K., Mackay, F., Strasser, A., et al. (2013). Mcl-1 is essential for the survival of plasma cells. *Nat. Immunol.* *14*, 290–297.
- Purtha, W.E., Tedder, T.F., Johnson, S., Bhattacharya, D., and Diamond, M.S. (2011). Memory B cells, but not long-lived plasma cells, possess antigen specificities for viral escape mutants. *J. Exp. Med.* *208*, 2599–2606.
- Rozanski, C.H., Arens, R., Carlson, L.M., Nair, J., Boise, L.H., Chanan-Khan, A.A., Schoenberger, S.P., and Lee, K.P. (2011). Sustained antibody responses depend on CD28 function in bone marrow-resident plasma cells. *J. Exp. Med.* *208*, 1435–1446.
- Salabei, J.K., Gibb, A.A., and Hill, B.G. (2014). Comprehensive measurement of respiratory activity in permeabilized cells using extracellular flux analysis. *Nat. Protoc.* *9*, 421–438.
- Scaduto, R.C., Jr., and Grotyohann, L.W. (1999). Measurement of mitochondrial membrane potential using fluorescent rhodamine derivatives. *Biophys. J.* *76*, 469–477.
- Schaffer, J.E., and Lodish, H.F. (1994). Expression cloning and characterization of a novel adipocyte long chain fatty acid transport protein. *Cell* *79*, 427–436.
- Schlierf, G., and Dorow, E. (1973). Diurnal patterns of triglycerides, free fatty acids, blood sugar, and insulin during carbohydrate-induction in man and their modification by nocturnal suppression of lipolysis. *J. Clin. Invest.* *52*, 732–740.
- Shaffer, A.L., Shapiro-Shelef, M., Iwakoshi, N.N., Lee, A.H., Qian, S.B., Zhao, H., Yu, X., Yang, L., Tan, B.K., Rosenwald, A., et al. (2004). XBP1, downstream of Blimp-1, expands the secretory apparatus and other organelles, and increases protein synthesis in plasma cell differentiation. *Immunity* *21*, 81–93.
- Shapiro-Shelef, M., Lin, K.I., Savitsky, D., Liao, J., and Calame, K. (2005). Blimp-1 is required for maintenance of long-lived plasma cells in the bone marrow. *J. Exp. Med.* *202*, 1471–1476.
- Shi, W., Liao, Y., Willis, S.N., Taubenheim, N., Inouye, M., Tarlinton, D.M., Smyth, G.K., Hodgkin, P.D., Nutt, S.L., and Corcoran, L.M. (2015). Transcriptional profiling of mouse B cell terminal differentiation defines a signature for antibody-secreting plasma cells. *Nat. Immunol.* *16*, 663–673.
- Slifka, M.K., Antia, R., Whitmire, J.K., and Ahmed, R. (1998). Humoral immunity due to long-lived plasma cells. *Immunity* *8*, 363–372.
- Smith, K.G., Weiss, U., Rajewsky, K., Nossal, G.J., and Tarlinton, D.M. (1994). Bcl-2 increases memory B cell recruitment but does not perturb selection in germinal centers. *Immunity* *1*, 803–813.
- Sze, D.M., Toellner, K.M., García de Vinuesa, C., Taylor, D.R., and MacLennan, I.C. (2000). Intrinsic constraint on plasmablast growth and extrinsic limits of plasma cell survival. *J. Exp. Med.* *192*, 813–821.
- Tooze, R.M. (2013). A replicative self-renewal model for long-lived plasma cells: questioning irreversible cell cycle exit. *Front. Immunol.* *4*, 460.
- Tung, J.W., Parks, D.R., Moore, W.A., Herzenberg, L.A., and Herzenberg, L.A. (2004). New approaches to fluorescence compensation and visualization of FACS data. *Clinical immunology* *110*, 277–283.
- van Anken, E., Romijn, E.P., Maggioni, C., Mezghrani, A., Sitia, R., Braakman, I., and Heck, A.J. (2003). Sequential waves of functionally related proteins are expressed when B cells prepare for antibody secretion. *Immunity* *18*, 243–253.
- van der Windt, G.J., Everts, B., Chang, C.H., Curtis, J.D., Freitas, T.C., Amiel, E., Pearce, E.J., and Pearce, E.L. (2012). Mitochondrial respiratory capacity is a critical regulator of CD8+ T cell memory development. *Immunity* *36*, 68–78.
- van Spruiel, A.B., de Keijzer, S., van der Schaaf, A., Gartlan, K.H., Sofi, M., Light, A., Linssen, P.C., Boezeman, J.B., Zuidschermwoude, M., Reinieren-Beeren, I., et al. (2012). The tetraspanin CD37 orchestrates the $\alpha(4)\beta(1)$ integrin-Akt signaling axis and supports long-lived plasma cell survival. *Sci. Signal.* *5*, ra82.
- Vander Heiden, M.G., Plas, D.R., Rathmell, J.C., Fox, C.J., Harris, M.H., and Thompson, C.B. (2001). Growth factors can influence cell growth and survival through effects on glucose metabolism. *Mol. Cell. Biol.* *21*, 5899–5912.
- Vigueira, P.A., McCommis, K.S., Schweitzer, G.G., Remedi, M.S., Chambers, K.T., Fu, X., McDonald, W.G., Cole, S.L., Colca, J.R., Kletzien, R.F., et al. (2014). Mitochondrial pyruvate carrier 2 hypomorphism in mice leads to defects in glucose-stimulated insulin secretion. *Cell Rep.* *7*, 2042–2053.

Weisel, F.J., Zuccarino-Catania, G.V., Chikina, M., and Shlomchik, M.J. (2016). A Temporal Switch in the Germinal Center Determines Differential Output of Memory B and Plasma Cells. *Immunity* 44, 116–130.

Woodland, R.T., Fox, C.J., Schmidt, M.R., Hammerman, P.S., Opferman, J.T., Korsmeyer, S.J., Hilbert, D.M., and Thompson, C.B. (2008). Multiple signaling pathways promote B lymphocyte stimulator dependent B-cell growth and survival. *Blood* 111, 750–760.

Yoshioka, K., Saito, M., Oh, K.B., Nemoto, Y., Matsuoka, H., Natsume, M., and Abe, H. (1996). Intracellular fate of 2-NBDG, a fluorescent probe for glucose uptake activity, in *Escherichia coli* cells. *Biosci. Biotechnol. Biochem.* 60, 1899–1901.

Zelle, R.M., Harrison, J.C., Pronk, J.T., and van Maris, A.J. (2011). Anaplerotic role for cytosolic malic enzyme in engineered *Saccharomyces cerevisiae* strains. *Appl. Environ. Microbiol.* 77, 732–738.